Proc. of the Second Intl. Conf. on Advances in Information Processing and Communication Technology - IPCT 2015

ISBN: 978-1-63248-044-6 doi: 10.15224/ 978-1-63248-044-6-78

SIMULATIONS OF THE RAYLEIGH-BÉNARD CONVECTION TYPE ACOUSTIC STREAMING MOTION IN ACOMPRESSIBLE GAS FILLED TWO-DIMENSIONAL RECTANGULAR ENCLOSURE

Kherief Nacereddine Mohamed, K. Talbi and F.Berrahil

ABSTRACT.

Rayleigh–Bénard convection is a fundamental phenomenon found in many atmospheric and industrial applications. Many numerical methods have been applied to analyze this problem. The effects of oscillatory flow structures on transient convective heat transfer in an air-filled shallow enclosure with a vibrating side wall are investigated. Oscillatory flows and Rayleigh-Bénard convection have been extensively studied. In the present study, fluid motion is driven by the periodic vibration of the enclosure side wall. The vertical walls of enclosure are adiabatic while the bottom wall is isothermally heated and the top wall is kept at an initial temperature. The fully compressible forms of the Navier-Stokes and energy equations are considered to compute the interaction of oscillatory and gravitational flow fields. A finite-volume method based, explicit time-marching Flux-Corrected Transport Algorithm is used to simulate the transport phenomena in the enclosure. The results of a test case simulation with stationary walls are compared with the existing literature for the validation of the algorithm utilized. The oscillatory fluid motion significantly changes the transient behavior of the thermal transport in the enclosure compared to the pure Rayleigh-Bénard convection.

Keywords: *Rayleigh-Bénard convection, periodic vibration, finite volume*

1. INTRODUCTION

A pressure wave field in a fluid can generate a secondary, steady circulatory flow termed as acoustic streaming. Acoustic streaming can enhance heat transfer and mixing. The acoustic streaming phenomenon has been extensively studied by using theoretical and experimental methods. However, the investigations on irregular acoustic streaming structures and effect of various parameters on irregular streaming are relatively scarce. Merkli and Thomann [1] observed irregular circulations in a Stokes layer resulting from the transition to turbulence and obtained a critical Reynolds number (with present nomenclature, $2u_{max}/(\nu\omega)^{1/2}\approx400$). Kawahashi and Arakawa [2] numerically studied acoustic streaming in a closed duct. They predicted shock wave propagation due to finite amplitude oscillations and distortion of the streaming structures. Yano [3] performed computational study of acoustic streaming formed by resonant oscillations with shock waves in a gas filled tube. For high streaming Reynolds numbers, irregular streaming patterns having vortices of various scales were predicted. Menguy and Gilbert [4] presented a comparison of slow and nonlinear acoustic streaming. The study focused on the distortion of the streaming field due to fluid inertia. A perturbation calculation using asymptotic expansions was performed and the unsymmetrical pattern of fast streaming was demonstrated. Alexeev and Gutfinger [5] investigated the periodic gas oscillations in closed tubes experimentally and numerically. They reported shock waves propagating along the tube.

Aktas and Farouk [6] carried out a computational study to determine the influence of the wave form on streaming patterns in a two dimensional enclosure. For sharp pressure gradients, irregular streaming patterns were predicted. The influence of temperature gradients on acoustic streaming flows has been studied by several researchers. Thompson

Kherief Nacereddine Mohamed Docteur
Ecole supérieur d'enseignement technique Skikda
Algeria

K. Talbi Professeur,
Université Mentouri Constantine faculté des sciences de l'ingénieur département de Génie mécanique.
Algeria

F. Berrahil Docteur,
Université Mila faculté des sciences de l'ingénieur département de Génie mécanique.
Algeria

Proc. of the Second Intl. Conf. on Advances in Information Processing and Communication Technology - IPCT 2015

ISBN: 978-1-63248-044-6 doi: 10.15224/ 978-1-63248-044-6-78

and Atchley [7] conducted acoustic and streaming velocity measurements in an air-filled cylindrical resonator by employing laser Doppler anemometry technique. Using this experimental method, Thompson et al. [8] investigated the effects of a thermoacoustically induced axial temperature gradient and fluid inertia on the acoustic streaming generated in the resonator. A strong dependence between the temperature gradient and the streaming structures was reported. The streaming velocities decrease with increasing temperature gradient and the distortion of the streaming patterns is observed. Murat K. Aktas [9] studied the irregular acoustic streaming in symmetrically heated (for horizontal walls) rectangular enclosures. A parametric study is performed in order to evaluate the effect of wall displacement amplitude, enclosure height and wall temperature on transport phenomena in the enclosure.

Due to its practical importance in many general science and engineering applications, Rayleigh–Bénard convection has been the subject of many theoretical, experimental, and numerical studies. Since Rayleigh–Bénard convection presents the evolution from the stationary state to the fully developed turbulent regime with many different flow patterns and sequences of bifurcations, it is widely investigated as the problems of different transition mechanisms in hydrodynamics [10–13].

In Rayleigh–Bénard convection, the primary instability, which represents a transition from diffusive thermal conduction to stationary time-independent steady convection with a structure of steady 2D rolls, occurs at a critical Rayleigh number of Ra_c = 1707,76 for the case of no-slip boundary conditions imposed on solid walls. The value of this critical Rayleigh number is independent of the Prandtl number. However, as the Rayleigh number increases, a bifurcation to a time-dependent flow structure with a single-frequency periodic state is observed, namely the secondary instability. This transition to the secondary instability is strongly dependent on the Prandtl number.

Moreover, as the Rayleigh number is increased further, two-frequency quasi-periodic flow is generated from the single-frequency oscillatory state and the flow finally transits to a chaotic state in the fully developed turbulent regime. Early experimental results for the transition to turbulence in Rayleigh–Bénard convection were presented by Krishnamurti [14].

For a three-dimensional, incompressible flow heated from below, bifurcation patterns for different Prandtl numbers were investigated numerically by Bucchignani and Stella [15]. Semih and Murat [16] studied the effects of oscillatory fluid motion on Rayleigh-Bénard convection in a rectangular enclosure was investigated.

In this study, they also examined the transition from oscillatory behavior to the chaotic behavior for the same geometry and flow characteristics. In these studies, incompressible Newtonian fluid was analyzed by employing the Boussinesq approximation. In the present study, the effects of oscillatory fluid motion on Rayleigh-Bénard convection in a rectangular enclosure are investigated.

The predictions of flow structure and the temperature values for the pure Rayleigh-Bénard convection were compared with the literature to validate the numerical methodology that was used. The interaction of the oscillatory flow field and Rayleigh-Bénard convection cells were simulated and the augmentation of heat transfer from the bottom wall was evaluated.

2. MATERIAL AND METHODOLOGY

A two-dimensional shallow enclosure filled with air is considered Figure 1. The enclosure height is 10 mm and the length is 40 mm. Corresponding aspect ratio of the enclosure is 4. Air is heated from the below by T_h temperature and cooled from above by T_c temperature and the vertical walls of enclosure are adiabatic.

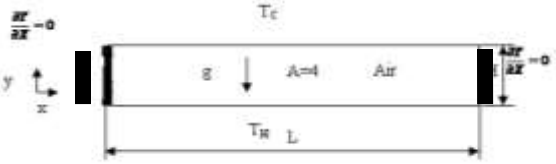

Figure 1. Problem geometry and corresponding boundary conditions.

No-slip boundary condition was implemented for all solid walls. The oscillatory motion of air is driven by the harmonic vibration of the left wall at certain frequency. The frequency of wall is chosen as to create a standing wave at the first fundamental mode in the enclosure in order to maximize the pressure wave amplitudes and oscillatory flow velocities.

2.1 Interaction of mechanically driven heat transfer in a closed rectangular chamber:

A sound field is formed by a series of compressions and expansions of a substance, which obey the laws of thermodynamics, heat transfer, and fluid mechanics. It is essentially characterized by the pressure p, corresponding density ρ, temperature T, and velocities. Hence, an accurate mathematical model must be able to describe the compressible behavior of the substance in question. In this study, the compressible form of the Navier-Stokes equations in 2-D Cartesian coordinate system, including the conservation of mass, momentum and energy, along with a state equation, are used as the governing equations:

$$\frac{\partial \rho}{\partial t} + \frac{\partial(\rho u)}{\partial x} + \frac{\partial(\rho v)}{\partial y} = 0 \quad (1)$$

$$\rho\frac{\partial u}{\partial t} + \rho u\frac{\partial u}{\partial x} + \rho v\frac{\partial u}{\partial y} = -\frac{\partial P}{\partial x} + \left[\frac{\partial \tau_{xx}}{\partial x} + \frac{\partial \tau_{xy}}{\partial y}\right] \quad (2)$$

$$\rho\frac{\partial v}{\partial t} + \rho u\frac{\partial v}{\partial x} + \rho v\frac{\partial v}{\partial y} = -\frac{\partial P}{\partial y} + \left[\frac{\partial \tau_{yy}}{\partial y} + \frac{\partial \tau_{xy}}{\partial x}\right] \quad (3)$$

$$\frac{\partial E}{\partial t} + \frac{\partial}{\partial x}\left[(E+p)u\right] + \frac{\partial}{\partial y}\left[(E+p)v\right] = \frac{\partial}{\partial x}\left[u\tau_{xx} + v\tau_{xy}\right] + \frac{\partial}{\partial y}\left[u\tau_{xy} + v\tau_{yy}\right] - \frac{\partial q_x}{\partial x} - \frac{\partial q_y}{\partial y} \quad (4)$$

The effect of gravity is not considered in the present numerical simulations. Here

Proc. of the Second Intl. Conf. on Advances in Information Processing and Communication Technology - IPCT 2015

ISBN: 978-1-63248-044-6 doi: 10.15224/ 978-1-63248-044-6-78

$$E = \frac{P}{\gamma - 1} + \frac{1}{2}\rho\left(u^2 + v^2\right) \quad (5)$$

The components of the stress tensor τ are:

$$\tau_{xx} = \frac{4}{3}\mu\frac{\partial u}{\partial x} - \frac{2}{3}\mu\frac{\partial v}{\partial y} \quad (6)$$

$$\tau_{yy} = \frac{4}{3}\mu\frac{\partial v}{\partial y} - \frac{2}{3}\mu\frac{\partial u}{\partial x} \quad (7)$$

$$\tau_{yx} = \tau_{xy} = \mu\frac{\partial u}{\partial y} + \mu\frac{\partial v}{\partial x} \quad (8)$$

where μ is the shear viscosity. The components of the heat-flux vector are written as:

$$q_x = -k\frac{\partial T}{\partial x} \qquad q_y = -k\frac{\partial T}{\partial y}$$

where k is thermal conductivity and T is temperature. The ideal gas law is;

$$p = \rho RT \quad (9)$$

Where R=287 J/kgK is the gas constant of air.

The finite-volume method is used for the numerical resolution the system of transport equations:

$$\frac{\partial \phi}{\partial t} + \frac{\partial (U_i \phi)}{\partial X_i} + \frac{\partial}{\partial X_i}(D_1) = C_2\frac{\partial D_2}{\partial X_i} + D_3 \quad (10)$$

Where U_i is the local convection velocity, D1, D2, and D3 are additional source terms. The quantity Φ can be any flow variable, such as density ρ, momentum flux (ρu, ρv, ρw) or energy E. The value C2 can either be a constant or a function of convected variables.

The governing equations (except for the diffusion terms) are discretized using a finite-volume method based on the flux-corrected transport (FCT) algorithm. FCT is a high-order, nonlinear, monotone, conservative and positivity-preserving method designed to solve a general one-dimensional continuity equation with appropriate source terms.

This scheme has fourth-order phase accuracy and is able to resolve step gradients with minimum numerical diffusion. The diffusion terms (the viscous term in the momentum equations and the conduction terms in the energy equation) were discretized using a second-order central difference approach. Time-step splitting was also used to couple all of the representative physical effects.

No-slip boundary conditions were used at all solid walls. In the present computational method, the treatment proposed by Poinsot and Lele was followed for implementing the boundary conditions for the density.

Initial and Boundary Conditions

The boundary conditions of the problem under investigation are:

u(0,y,t) = v(0,y,t) = 0

u(L,y,t) = v(L,y,t) = 0 u(x,0,t) = v(x,0,t) = 0

u(x,H,t) = v(x,H,t) = 0 $\frac{\partial T}{\partial x}(0,y,t) = \frac{\partial T}{\partial y}(L,y,t) = 0$

$T(x,0,t) = T_h$ $T(x,H,t) = T_c$

The initial conditions are: p(x,y,0) = 101325 Pa; T(x,y,0) = 300 K; ρ(x,y,0) = 1.1768 kg/m^3

The boundary conditions for the higher order FCT-based solutions of the Navier-Stokes equations require a rigorous formulation. No-slip boundary conditions are used for velocity on all walls. The wall boundary conditions for density are updated using the formulation developed by Poinsot and Lele [17] based on characteristic wave relations. The use of this method avoids over-specification of variables and incorrect extrapolations from interior point values.

The stated equations in the previous section were solved by using a finite volume based explicit time marching flux corrected transport (FCT) algorithm. The reason behind using this algorithm for the numerical simulations lies in the fact that it has relatively higher ability to resolve steep gradients with minimum numerical diffusion. FCT is a high-order, nonlinear, monotone, conservative and positivity-preserving method designed to solve a general one-dimensional continuity equation with appropriate source terms. The diffusion terms (the viscous term in the momentum equations and the conduction terms in the energy equation) were discretized using a second-order central difference approach. Time-step splitting was also used to couple all of the representative physical effects. A more detailed discussion of FCT algorithm is performed by Oran and Boris [18].

As stated in the study of Tillet et al. [19], higher order, non-dissipative algorithms such as FCT, requires a great vigilance to prevent the spurious wave reflections in the vicinities of boundaries and nonphysical numerical oscillations arising from instabilities when the boundary conditions are being implemented. In present study, treatment proposed by Poinsot and Lele [17] is used to accurately compute the density along the stationary no-slip walls.

Since an algorithm based on explicit numerical method is employed, the CFL (Courant-Friedrichs- Lewy) stability condition is important. In order to satisfy the stability criteria the time step size of the computations was chosen based on:

$$\Delta t = (CFL) \times \left[\frac{\min(\Delta x, \Delta y)}{a_{i,j}}\right] \quad (11)$$

The selected CFL number for the analysis is 0.4 which is already smaller than the necessary value of 0.5. [16]

In the present numerical simulations typically 201 x 51 uniform numerical meshes are utilized to be small enough considering the computational time constraint for the enclosure having the height of 10 mm and length of 40 mm, respectively. The computations performed using even denser numerical mesh did not alter the results significantly as shown in the next section.

For the code validation purpose, the pure Rayleigh-Bénard convection predictions of Soong et al. [20] were

Proc. of the Second Intl. Conf. on Advances in Information Processing and Communication Technology - IPCT 2015

ISBN: 978-1-63248-044-6 doi: 10.15224/ 978-1-63248-044-6-78

used. In the aforementioned study, for A=4 and Ra=10000, the bottom and the top wall temperatures was taken as T_h=320 K and T_c=300 K, respectively ($\Delta T = 20K$). The dimensionless maximum velocity components u and v and Nu number was compared with the existing data. For the comparison of these parameters, length and velocity components are non-dimensionalized by H and α/H respectively. Nusselt number is calculated as:

$$Nu = \frac{\left(\frac{\partial T}{\partial Y}\right) \times H}{\Delta T} \quad (12)$$

Maximum velocity components and Nusselt numbers obtained from the base case simulation are presented in the Table 1.

Table 1. Comparisons of the obtained results with the literature.

	Nu [16]	*Nu Present Study*
191x46	2.09	2.23
201x46	2.11	2.45
201x51	2.12	2.49

The present numerical predictions agree quite well with literature. Soong et al. [20] employed Boussinesq approximation in their work. Since fully compressible formulation is employed in the present work v_{max} value slightly differs from the prediction of Soong et al.

v velocities at x=L/2.

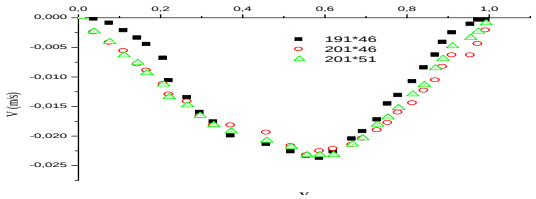

Figure 2. v-velocity values for different mesh configurations at x=L/2.

As it can be observed from Fig.2, using denser meshes in both height and length scale of the enclosure did not alter the results significantly. Effects of using different mesh structures on the bottom wall Nusselt numbers are also investigated and results are presented in Table 2.

Table 2. Comparison of Nusselt numbers for different mesh values.

	Soong et al. [1996]	*[16] Semih C. and Murat K.*	*Present Study*
u_{max}	16.1	16.2	16.0
v_{max}	18.0	19.7	20.2
Nu	2.1	2.12	2.17

It can be seen that using approximately 10% denser mesh in both x and y direction changes the bottom wall Nu number as 1.5 %.

Fig. 3 and Fig.4 depict the time evolution of the flow field and temperature distribution at different instants for the case of pure Rayleigh-Bénard convection. The flow field and corresponding temperature distribution are consistent with the literature.

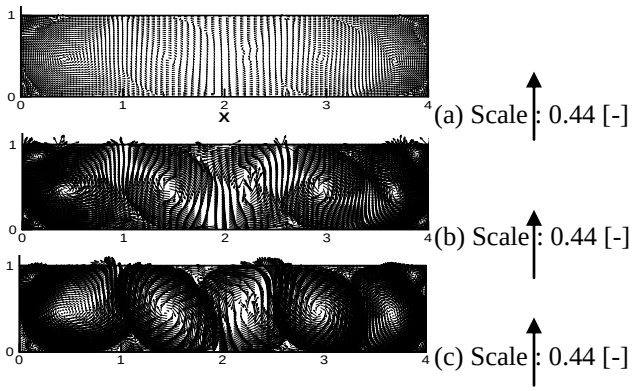

Figure 3. Velocity vectors for different instants for pure Rayleigh-Bénard convection (a) t=1.5 s, (b) t=3s, (c) t=5s.

At relatively early times (1.5 s) the velocity values are rather small while the characteristic nature of the Rayleigh-Bénard cells for A=4 starts to be established (Fig. 3a). At 3 s., the typical cell structure develops but the velocity values continue to increase further (Fig. 3b). At 5 s., the typical cell structure (Ga=10000) with two clock wise and three counter clock wise rotating vortices fully develops (Fig. 3c). The time evolution of the temperature distribution in the flow domain for pure Rayleigh-Bénard convection was presented in Fig.4. The diffusive transport dominates temperature field at early times (Fig. 4a). At 3 s., the characteristic temperature distribution in Rayleigh-Bénard for A=4 starts to be established (Fig. 4b). At 5 s., fully developed Rayleigh- Bénard convection cells are observed. The fully developed temperature field completely agrees with the results in the literature.

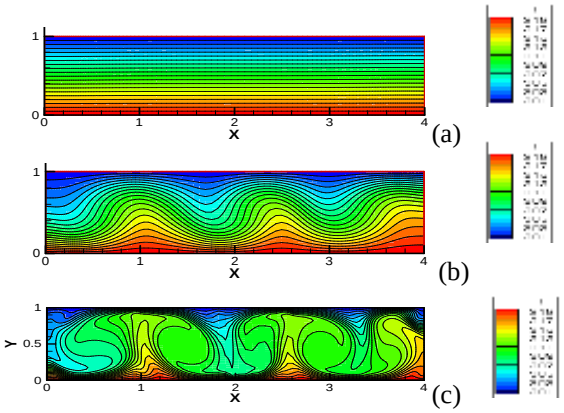

Figure 4. Temperature distribution for different instants for pure Rayleigh-Bénard convection at (a) t=1.5 s, (b) t=3 s, (c) t=5s.

2.2 Interaction of mechanically driven acoustic wave and heat transfer in a closed rectangular chamber:

The vibration frequency of the harmonic vibration of the enclosure is chosen as f= 2893 Hz. Four different maximum

Proc. of the Second Intl. Conf. on Advances in Information Processing and Communication Technology - IPCT 2015

ISBN: 978-1-63248-044-6 doi: 10.15224/ 978-1-63248-044-6-78

displacement values were considered. As a rule of thumb, particle velocity (velocity amplitude) should be equal to ratio of the pressure to specific acoustic impedance (Δp/Z) and the calculation, the specific acoustic impedance is taken as Z=413 (Ns/m3) for the air of T=20^{0}C. [16].

In the simulation of the oscillatory flow and Rayleigh-Bénard convection, the left wall of the enclosure is harmonically vibrated by the formula of $X = X_{max}\sin\omega t$

In the present study, ω (angular frequency) is selected as 18177 rad/s (f= 2893 Hz) and the maximum wall displacement is selected as 5μm, 3μm and 1μm.

In the two-dimensional Cartesian coordinate system, the N-S equations are expressed in the non-dimensional conservative form as:

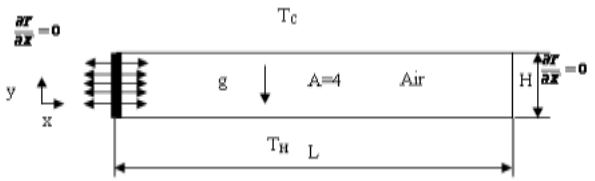

Figure 5. Problem geometry and corresponding boundary conditions.

$$St\frac{\partial\rho}{\partial t}+\frac{\partial(\rho u)}{\partial x}+\frac{\partial(\rho v)}{\partial y}=0 \quad (13)$$

$$St\frac{\partial(\rho u)}{\partial t}+\frac{\partial(\rho u^2)}{\partial x}+\frac{\partial(\rho uv)}{\partial y}=-\frac{\partial P}{\partial x}+\frac{1}{\mathrm{Re}}\left[\frac{\partial\tau_{xx}}{\partial x}+\frac{\partial\tau_{xy}}{\partial y}\right] \quad (14)$$

$$St\frac{\partial(\rho v)}{\partial t}+\frac{\partial(\rho uv)}{\partial x}+\frac{\partial(\rho v^2)}{\partial y}=-\frac{\partial P}{\partial y}+\frac{1}{\mathrm{Re}}\left[\frac{\partial\tau_{yy}}{\partial y}+\frac{\partial\tau_{xy}}{\partial x}\right] \quad (15)$$

$$\frac{\partial E}{\partial t}+\frac{\partial(Eu)}{\partial x}+\frac{\partial(Ev)}{\partial y}+(\gamma-1)\left[\frac{\partial(pu)}{\partial x}+\frac{\partial(pv)}{\partial y}\right]=\frac{\gamma}{\mathrm{Pr}^*\mathrm{Re}}\left(-\frac{\partial q_x}{\partial x}-\frac{\partial q_y}{\partial y}\right)+\frac{\gamma Ec}{\mathrm{Re}}\phi \quad (16)$$

Here, St is Strouhal Number $St=\frac{\omega L}{u_0}$

Ec is Eckert Number $Ec=\frac{u_0^2}{c_pT_0}=(\gamma-1)M^2$ and the non-dimensional viscous dissipation is written as

$$\phi=\frac{\partial}{\partial x}\left[u\tau_{xx}+v\tau_{xy}\right]+\frac{\partial}{\partial y}\left[u\tau_{xy}+v\tau_{yy}\right] \quad (17)$$

The dimensionless variables are:

$$\begin{aligned}
&x=\frac{x^*}{L^*};\ y=\frac{y^*}{L^*};\ p=\frac{p^*-p_0^*}{\rho_0^*(u_0^*)^2};\\
&\rho=\frac{\rho^*}{\rho_0^*};\ T=\frac{T^*}{T_0^*};\ E=\frac{E^*}{E_0^*};\\
&u=\frac{u^*}{u_0^*};\ v=\frac{v^*}{v_0^*};\ \mu=\frac{\mu^*}{\mu_0^*};\\
&k=\frac{k^*}{k_0^*};\ c_p=\frac{c_p^*}{c_{p0}^*};\\
&c_v=\frac{c_v^*}{c_{v0}^*};\ t=t^*\omega^*.
\end{aligned} \quad (18)$$

Here, the variables with subscript 0 are the initial values. The quantity u_0* is wall vibration amplitude, and ω* is the angular frequency of wall vibration.

The fluid thermophysical properties in the dimensionless group, Re, St, Ec and Pr, are evaluated at the initial temperature, and the specialized velocity used is the maximum velocity of the left wall vibration.

Initial and Boundary Conditions

The boundary conditions of the problem under investigation are:

$u(0,y,t) = \omega X_{max}\cos\omega t$ $\quad$ $v(0,y,t) = 0$

$u(L,y,t) = v(L,y,t) = 0$ $\quad$ $u(x,0,t) = v(x,0,t) = 0$

$u(x,H,t) = v(x,H,t) = 0$

$$\frac{\partial T}{\partial x}(0,y,t)=\frac{\partial T}{\partial y}(L,y,t)=0$$

$T(x,0,t) = T_h$ $\quad$ $T(x,H,t) = T_c$

Fig.6 depicts that when the wall displacement value increases the amplitude of the pressure oscillations also increases both for the left wall. Stronger pressure waves drive stronger fluid motion in the enclosure. The enhancement of the flow velocity increases the convective heat transfer from the bottom wall.

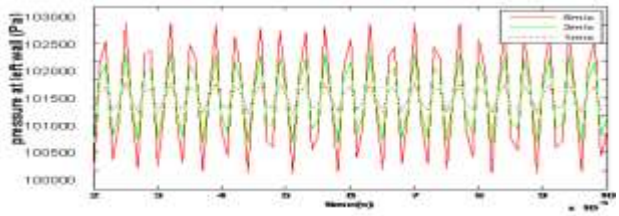

Figure 6. Time evolution of relative pressure wave amplitudes for different wall displacement values at the vicinity of t=0.01

The time averaged flow fields in the enclosure in the enclosure at 5 s are shown in Fig. 6 for different cases. By this time the time averaged velocities reach pseudo-steady values. The time averaging is applied to instantaneous velocity values for one period of wall vibration and pseudo-steady velocity values are obtained.

In Fig. 7a, the signature of the flow field is quite similar to that of pure Rayleigh-Bénard convection except the rotation direction of the cells. This pattern indicates a stronger flow field (due to oscillatory wall motion) which has similar to Bénard cells but has opposite flow direction.

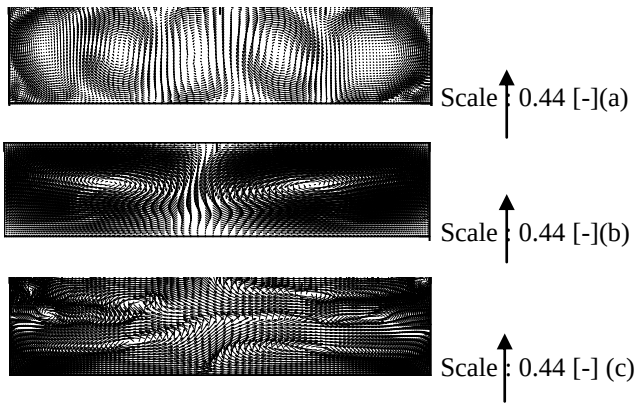

Figure 7. Cycle averaged velocity vectors for different wall displacement values (a) Xmax=1μm, (b) Xmax=3μm and (c) Xmax=5 μm.

Proc. of the Second Intl. Conf. on Advances in Information Processing and Communication Technology - IPCT 2015

ISBN: 978-1-63248-044-6 doi: 10.15224/ 978-1-63248-044-6-78

Fig.7 shows that below the wall displacement value 3 μm, the flow field significantly changes. Because of this alteration in the flow field, Nusselt number for these Xmax values significantly lower than the higher Xmax values explained in the Table 3 below.
Table 3 presents the Nusselt numbers from the bottom wall for these different maximum left wall displacement values.

Table 3. Average heat transfer from the bottom wall for different left wall displacement values.

Wall displacement	*Cycle averaged Nu number for the bottom wall at 5 s*
5 μm	25.84
3 μm	19.57
1 μm	8.29

3. CONCLUSIONS

This study performed a series of simulations of 2D Rayleigh-Bénard convection and an oscillatory flow in a differentially heated enclosure is numerically simulated.

The wall vibration driven flow effects Rayleigh-Bénard convection in a considerable extent and the oscillatory fluid motion significantly changes the transient behavior of heat transfer in the enclosure compared to Rayleigh-Bénard convection.

It is observed that with the increment in the left wall vibration, the flow field significantly differs from the classical Rayleigh-Benard convection cell structure and as a result of this; flow inside the enclosure apt to generate a secondary circulating motions. Furthermore, the last cycle averaged bottom wall Nusselt values increases proportional to the left wall displacements. It is observed that while the classical Rayleigh-Benard convection has a bottom Nu value of 8.29 (Ga=10000), when 5 μm amplitude of vibration is applied to the system, this value increases to 25.84 which is about the 4 times higher than the original value.

REFERENCES

[1] P. Merkli and H. Thomann, Transition to turbulence in oscillating pipe flow, J. Fluid Mech., vol. 68 (3), pp. 567–575, 1975.

[2] S. Moreau, H. Bailliet and J.C. Valiere, Measurements of inner and outer streaming vortices in a standing waveguide using laser doppler velocimetry, J. Acoust. Soc. Am., vol. 123 (2), pp. 640–647, 2008.

[3] M. Kawahashi and M. Arakawa, Nonlinear phenomena induced by finite-amplitude oscillation of air column in closed duct, JSME Int. J., vol. 39 (2), pp. 280–286, 1996.

[4] T. Yano, Turbulent acoustic streaming excited by resonant gas oscillation with periodic shock waves in a closed tube, J. Acoust. Soc. Am., vol. 106 (1), pp. L7–L12, 1999.

[5] A. Alexeev and C. Gutfinger, Resonance gas oscillations in closed tubes: Numerical study and experiments, Phys. Fluids, vol. 15 (11), pp. 3397–3408, 2003.

[6] M.K. Aktas and B. Farouk, Numerical simulation of acoustic streaming generated by finite-amplitude resonant oscillations in an enclosure, J. Acoust. Soc. Am., vol. 116 (5), pp. 2822–2831, 2004.

[7] M.W. Thompson and A.A. Atchley, Simultaneous measurement of acoustic and streaming velocities in a standing wave using laser Doppler anemometry, J. Acoust. Soc. Am., vol. 117 (4), pp. 1828–1838, 2005.

[8] M.W. Thompson, A.A. Atchley and M.J. Maccarone, Influences of a temperature gradient and fluid inertia on acoustic streaming in a standing wave, J. Acoust. Soc. Am. vol. 117 (4), pp. 1839–1849, 2005.

[9] Murat K. Aktas. [2012], Irregular Acoustic Streaming Formation in Symmetrically Heated Enclosures, Proceedings of the World Congress on Engineering 2012 Vol III WCE 2012, July 4 - 6, London, U.K.

[10] S. Chandrasekhar, 1961, Hydrodynamic and Hydromagnetic Stability, Clarendon Press, Oxford.

[11] R.M. Clever, F.H. Busse, (1974), Transition to time-dependent convection, J. Fluid Mech. 65 (4) 625–645.

[12] J.H. Curry, J.R. Herring, J. Loncaric, S.A. Orszag, (1984), Order and disorder in two- and three-dimensional Bénard convection, J. Fluid Mech. 147 1–38.

[13] R.E. Ecke, H. Haucke, Y. Maeno, J.C. (1986), Wheatley, Critical dynamics at a Hopf bifurcation to oscillatory Rayleigh–Be´nard convection, Phys. Rev. A 33 (3) 1870.

[14] R. Krishnamurti, (1973), some further studies on the transition to turbulent convection, J. Fluid Mech. 60 285–303.

[15] Stella F, Bucchignani E., [1999] Rayleigh-Benard convection in limited domains: Part 1-Oscillatory Flow, *Numerical Heat Transfer, Part A: Applications*, 36.1, pp. 1-16.

[16] Semih C. and Murat K. AKTAS, 2014, Interaction of rayleigh-bénard convection and oscillatory flows, Proceedings of CONV-14: Int. Symp. on Convective Heat and Mass Transfer June 8 – 13, Turkey.

[17] Poinsot T.J., Lele S.K., [1992] Boundary conditions for direct simulations of compressible viscous flows, *J. Comput. Phys*, *101* pp. 104–129.

[18] Oran E.S., Boris J. P., [2000] *Numerical simulation of reactive Flows*, Cambridge University Press, Cambridge, England.

[19] Tillet Saint-Martin, X. N. and Oran, E. S., [1997] Boundary conditions for FCT based solutions of the Navier-Stokes Equations, pp. 2-7, Navy Research Laboratory, Washington, DC.

[20] Soong C.Y., Tzeng P.Y., Chiang D.C., Sheu T.S., [1996] Numerical study on mode-transition of natural convection in differentially heated inclined enclosures, *Int. J. Heat Mass Transfer* 39, pp. 2869-2882.

NOMENCLATURE

α	Thermal diffusivity coefficient	m^2/s
A	Aspect ratio	L/H
β	Thermal expansion coefficient	K^{-1}
H	Height of enclosure	m
L	Length of enclosure	m
p	Dimensionless pressure	$P/\rho U^2$
R_a	Rayleigh number	$g\beta(Th-Tc)H^3/\alpha\nu$
M	Mach number	
Pr	Prandtl number	
Re	Reynolds number	
St	Strouhal Number	$\omega L/u_0$
Ec	Eckert Number	
F	frequency	
τ	Dimensionless time	$t\alpha/H^2$
U,V	Velocity components	m/s
u,v	Dimensionless vel. Comp	$U/(\alpha/H)$
ω	Angular frequency	$2\pi f$
τ	Dimensionless temp.	((T- Tc)/(Th-Tc))
x,y	Dimensionless coordinates	(X/H), (Y/H)
X	wall displacement	
γ	ratio of specific heat	
cp	specific heat at constant pressure	
cv	specific heat at constant volume	